



Optical properties of an octadecylphosphonic acid self-assembled monolayer on a silicon wafer

H.-Y. Nie ^{a,*}, N.S. McIntyre ^a, W.M. Lau ^a, J.M. Feng ^b

^a Surface Science Western, Room G-1, WSC, The University of Western Ontario, London, Ontario, Canada, N6A 5B7

^b Application Division, Nanometrics Japan Ltd., 8-9-5 Nishi-Gotanda, Shinagawa, Tokyo 141-0031, Japan

ARTICLE INFO

Article history:

Received 2 June 2008

Received in revised form 7 September 2008

Accepted 10 September 2008

Available online 14 September 2008

Keywords:

Ellipsometry and reflectometry

Atomic force microscopy

Self-assembled monolayers

Octadecylphosphonic acid

Silicon wafer

ABSTRACT

We report a study of a full-coverage octadecylphosphonic acid (OPA or ODP) self-assembled monolayer (SAM) spin-coated on the native oxide layer (SiO₂) of a single crystalline silicon (c-Si) wafer using spectroscopic ellipsometry (SE) and reflectometry (SR). The OPA SAM showed characteristics of being a dielectric film in visible range and becoming absorbing in deep-UV range. By assuming an optical stack model of OPA/SiO₂/c-Si for the OPA monolayer system and adopting the parameterized Tauc–Lorentz dispersion model, we obtained an excellent fit of the model to the SE and SR data, from which dispersion of optical functions as well as thickness of the OPA film were deduced. The OPA film thickness measured by atomic force microscopy (AFM) on partial coverage OPA samples was used as the initial trial film thickness in the fitting processes. The deduced OPA film thickness from SE and SR data fitting was in good agreement with that obtained by AFM.

© 2008 Elsevier B.V. All rights reserved.

1. Introduction

Organic molecular self-assembled monolayers (SAMs) prepared on a solid surface is a unique system for surface engineering [1]. Certain interaction strengths between the molecular headgroup and the substrate are required for SAM formation from a solution of the molecules of interest. This is manifested by the two predominately studied SAMs of alkanethiol on gold surfaces and alkylsilane on oxide surfaces [2,3], for which the strong S–Au bond and polymerization of silanol groups are responsible, respectively. On the other hand, lack of such interaction strengths is likely to prevent SAM formation, which has been demonstrated in the case of octadecylphosphonic acid (OPA or ODP) prepared on the native oxide layer (SiO₂) of silicon wafers when using a polar solvent [4–6]. This inability to form an OPA monolayer on SiO₂ is attributed to the fact that the interaction between the OPA headgroup and the silicon oxide is even weaker than interactions among the OPA molecules themselves [6].

However, recently, a method that promotes exclusively the headgroup–substrate interaction has been developed for delivery of weakly-bonded OPA SAMs onto SiO₂ covered silicon wafers via use of appropriate non-polar solvents having a dielectric constant near 4, such as trichloroethylene (TCE) and chloroform [6]. The driving force behind this method appears to be the alignment and concentration of the polar OPA molecular headgroup at the non-polar medium surface, reducing the activation energy of OPA SAM formation on a hydrophilic substrate. The OPA SAM formed on SiO₂ is terminated by ordered

methyl groups and closely-packed methylene chains, both of which are similar to well known silane SAMs on an oxide surface. We have demonstrated that the molecules in this weakly-bonded OPA/SiO₂ system are liable to manipulation by a positively-biased probe tip [7]; this may lead to applications of the system as a masking film for nanolithography or as a patterned dielectric film for molecular electronics applications on a silicon wafer. Understanding the optical properties of the OPA SAMs on SiO₂ is essential for these possible applications; however, no such data have been available for the OPA monolayer film.

Spectroscopic ellipsometry (SE) has proven effective for accessing the optical properties and the thickness of a thin inorganic or organic film prepared on a suitable substrate in a sensitive, precise, and nondestructive fashion [8–16]. SE measures the two ellipsometric parameters Δ and Ψ , which represent, respectively, the phase change of and the arctangent of amplitude ratio of the electric field between the components of a monochromatic light polarized parallel (p) and perpendicular (s) to the plane of incidence. For an isotropic film on an isotropic substrate, these two measurable ellipsometric parameters are related to the ratio of complex Fresnel reflection coefficients (r_p and r_s) for p- and s-polarized components by $\rho = r_p/r_s = \tan(\Psi) \cdot \exp(i\Delta)$. For optical systems of a film on a substrate, this ratio is a function of the optical functions of the film and the substrate, the thickness of the film, and wavelength and incident angle of the probe light beam. Therefore, fitting an appropriate dispersion model to the SE data allows a determination of the thickness and dispersion of optical functions, i.e., index of refraction n and extinction coefficient k for the film as a function of the probe light wavelength. Moreover, spectroscopic reflectometry (SR) measures the reflectance [17] of a monochromatic,

* Corresponding author.

E-mail address: hnie@uwo.ca (H.-Y. Nie).

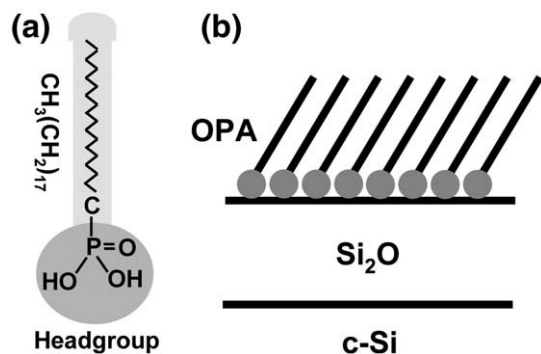


Fig. 1. Schematics for (a) an OPA molecule and (b) an OPA monolayer on the native SiO_2 layer of a single crystalline silicon wafer.

unpolarized, light from the sample surface. Because the reflectance measurement provides another set of data involving the same film thickness and optical functions, simultaneous SE and SR analyses thus serve to render a more confident estimation of the optical functions and film thickness than does SE alone [13].

We report in this paper our results on estimating dispersion of the optical functions and the thickness of a full-coverage OPA SAM spin-coated on SiO_2 covered single crystalline silicon (c-Si) wafer. In order to lend credence to our analyses, we measured the OPA monolayer thickness carefully using atomic force microscopy (AFM) on partial coverage OPA samples for the initial trial film thickness in the fitting procedures and comparisons with the deduced thickness from fitting an optical dispersion model to SE and SR data. Another step taken to enhance the confidence of the fitting processes was to simultaneously model multi-sets of data collected on different spots on both the OPA sample and the reference substrate.

2. Experimental and fitting procedures

Samples of OPA [$\text{CH}_3(\text{CH}_2)_{17}\text{P}(=\text{O})(\text{OH})_2$] monolayer were prepared by spin-coating a 2 mM OPA solution in TCE onto n-type Si (100) wafers cleaned by UV/ozone treatment for one hour. As silicon wafers inherently have native oxide layer (SiO_2) covering the c-Si substrate, the OPA monolayers were thus formed on SiO_2 . One of such silicon wafers without OPA coating was used as the reference substrate for SE and SR measurements. Schematics for an OPA molecule and the OPA monolayer on a silicon wafer are illustrated in Fig. 1a and b, respectively. When fully extended as illustrated in Fig. 1a, OPA molecules are believed to have a length of 2.5 nm [18]. The details for forming full-coverage OPA SAMs including the preparation of the OPA solution in TCE have been described elsewhere [6]. Contact mode of a Park Systems XE-100 AFM was used to measure the thickness of the monolayer from partial coverage samples. Silicon cantilevers with a spring constant of ~ 0.1 N/m were used. All images (256×256 pixels) were obtained in air at room temperature under a relative humidity of $\sim 40\%$.

SR and SE measurements on a full-coverage OPA on $\text{SiO}_2/\text{c-Si}$ as well as a reference substrate (i.e., $\text{SiO}_2/\text{c-Si}$), which was cut from the same wafer and witnessed the surface cleaning processes, were carried out using a Nanospec-9100DUVSE (Nanometrics, Milpitas, CA). The SR lamps (a deuterium arc lamp and a halogen lamp covering wavelength 192–370 nm and 370–780 nm, respectively) are focused into array detectors to select the operating wavelengths ranging 192–780 nm to measure the reflectance (ratio of the intensity of the reflected light to the incident) at a $15 \mu\text{m} \times 15 \mu\text{m}$ size spot. For SE, however, a Xe lamp, a monochromator, a non-rotating polarizer and a rotating compensator provide the monochromatic, polarized, light beam with a wavelength of 245–1000 nm. This light beam undergoes changes in polarization state upon reflection from the sample surface

at the same spot as for SR but with a larger area of $70 \mu\text{m} \times 50 \mu\text{m}$. These changes are analyzed using a non-rotating analyzer and an array CCD detector system. The angles of incidence for SE and SR are 65° and 11.2° with a $15\times$ lens, respectively. Three spots on each of the OPA sample and the $\text{SiO}_2/\text{c-Si}$ reference substrate were measured at room temperature with a controlled relative humidity less than 50%. SE and SR measurements were sequentially conducted within a couple of seconds.

To deduce the optical functions (n and k) and the thickness of the OPA film, an appropriate optical model is adopted with trial film thickness and optical functions to calculate Δ , Ψ and reflectance to fit the SE and SR data with a regression algorithm using a software package from J. A. Woollam Co. (WVASE32). Fitting for three sets of data (i.e., Δ , Ψ and reflectance) collected from three spots on the surface of the OPA sample were simultaneously performed assuming the same optical functions for the OPA film everywhere, the native SiO_2 layer and the c-Si substrate. The thickness of the SiO_2 layer was deduced from the SR and SE data from the reference $\text{SiO}_2/\text{c-Si}$ substrate and was coupled in the fitting process for the OPA film sample. The least square regression fitting procedure was repeated until the best-fit parameters were achieved in terms of their 90% confidence limits by minimizing the unbiased

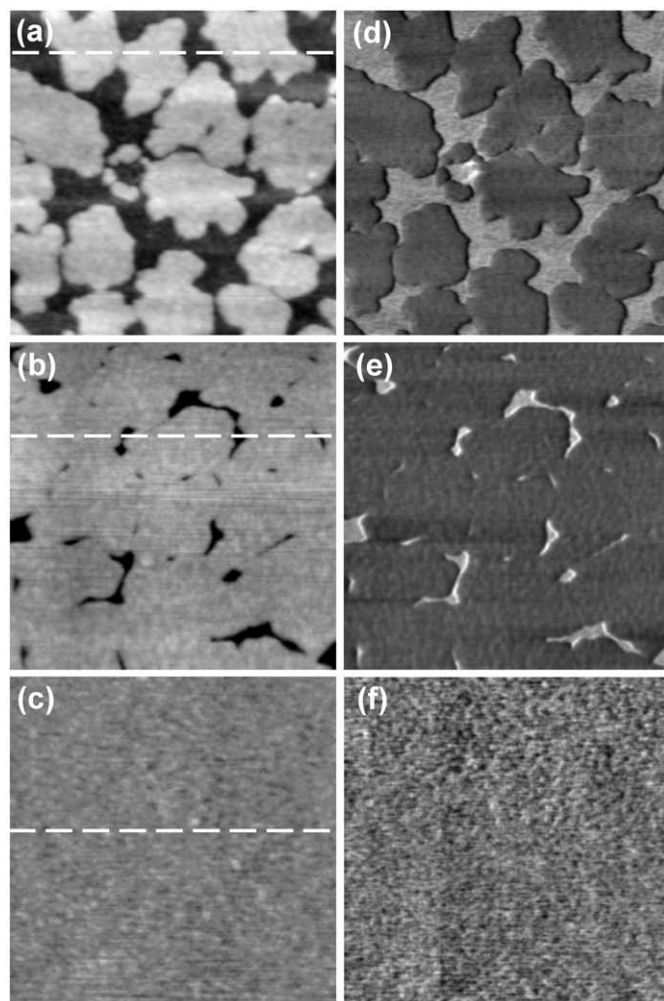


Fig. 2. AFM topographic images (scan area: $2 \mu\text{m} \times 2 \mu\text{m}$) for three OPA samples prepared on the native SiO_2 of a single crystalline silicon wafer with increasing coverage (a, b, up to 100% (c)). The inserted dashed lines in (a)–(c) show the location where a profile is isolated and shown in Fig. 3. Shown in (d)–(f) are friction force images corresponding to (a)–(c), respectively. The gray scale range for the topographic image from (a) to (c) is 3.0, 2.9, and 0.7 nm, respectively.

estimator mean squared error (MSE) of the mean square deviation [10,11],

$$\text{MSE} = \frac{1}{N-M} \sum \left[\frac{y_i^{\text{mod}} - y_i^{\text{exp}}}{\sigma_i} \right]^2 \quad (1)$$

where N is the number of independently measured values corresponding to different wavelengths and M the number of unknown model parameters. Here y^{mod} , y^{exp} and σ refer to model calculated values, experimental data and standard deviation of measured data, respectively.

3. Results and discussion

Fig. 2 shows AFM topographic and friction force images for OPA SAMs prepared on $\text{SiO}_2/\text{c-Si}$ with three different coverage, which were obtained by applying increasing amount of OPA solution in TCE onto the substrate. The additive nature of the OPA monolayer forming on SiO_2 can be used to control the monolayer coverage. Because only a partial coverage film allows AFM to measure the monolayer thickness, we show in Fig. 2a and b two such AFM images for monolayer thickness measurement. As shown in Fig. 2d and e, the partial-coverage samples also allow friction force imaging to distinguish the methyl terminated, hydrophobic, OPA monolayer and the exposed, hydrophilic, SiO_2 surface. Those friction force images show that the exposed SiO_2 surface has stronger interactions with the AFM tip, which is hydrophilic as the silicon tip is covered by its native oxide. For a full-coverage monolayer, as shown in Fig. 2c and f, the surface is featureless both in morphology and friction force, because now the surface is terminated by methyl groups. The average surface roughness for the full-coverage OPA film is ~ 0.06 nm; this is comparable to that of the underlying SiO_2 surface of the mirror-polished silicon wafer. Such a full-coverage OPA monolayer sample was used for the SE and SR experiment.

Shown in Fig. 3 are profiles isolated from the AFM images shown in Fig. 2a–c as indicated by the inserted dashed lines. These OPA monolayer samples were imaged immediately after OPA SAMs were prepared on the substrate to minimize possible adsorption of airborne contamination such as hydrocarbons onto the exposed SiO_2 surfaces, which is hydrophilic and has high surface energy. Apparently, there is no such a problem for a full-coverage OPA SAM sample, where the high surface energy SiO_2 surface becomes unavailable. These OPA

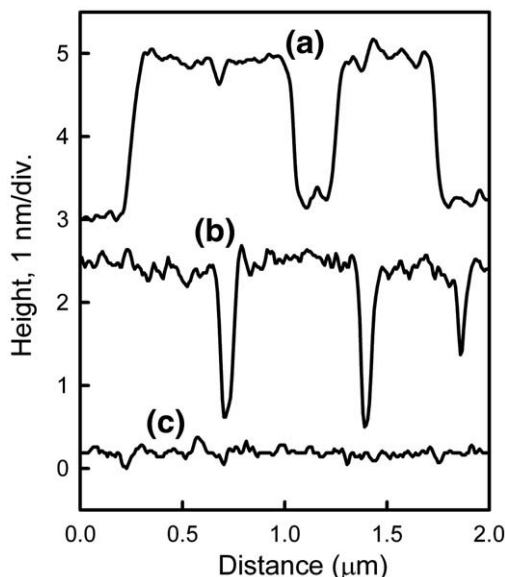


Fig. 3. Profiles a, b, and c isolated from images shown in Fig. 2a–c, respectively, for the three OPA samples with increasing coverage.

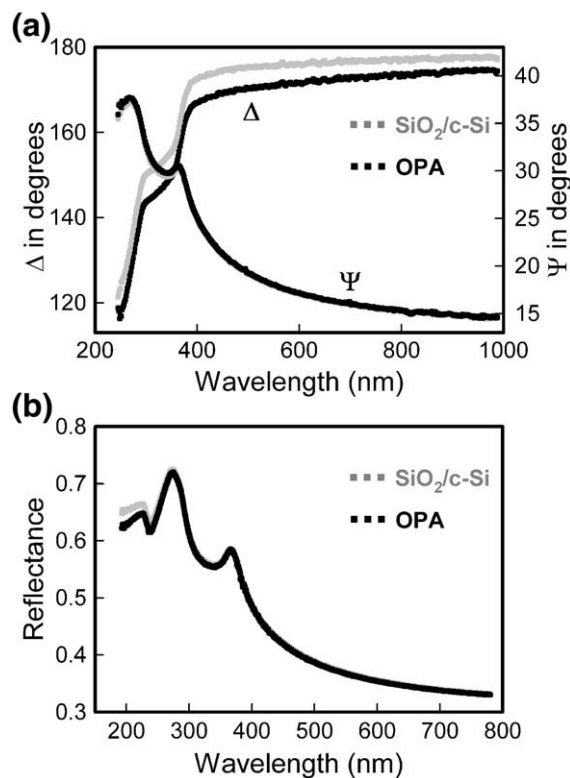


Fig. 4. One of the three sets of (a) Δ and Ψ data measured from a probe light beam with wavelength ranging from 245 to 1000 nm and (b) reflectance data measured from a different probe light beam with wavelength ranging from 192 to 780 nm on a full-coverage OPA sample (black) and a reference silicon wafer (grey).

samples were imaged with contact mode AFM, immediately upon preparation of the OPA film using applied forces of ~ 1 nN. Under those careful arrangements, the height for the partial-coverage OPA SAMs freshly prepared on a SiO_2 substrate is estimated to be 1.9 ± 0.1 nm. As a fully extended OPA molecule is 2.5 nm in length [18], OPA molecules in the SAM on SiO_2 must be tilted, as schematically illustrated in Fig. 1b.

We noticed that for aged samples the OPA monolayer height becomes less than that of the fresh ones, most likely due to adsorption of airborne contaminants on the exposed SiO_2 surface. Furthermore, because AFM is a mechanical probe technique relying on interactive forces between the probe tip and the sample surface to image the surface morphology, forces applied to the sample surface may impact the outcome of the height measurement, especially for flexible organic molecular layers like the OPA SAMs. When operated under large amplitudes, the dynamic force mode AFM could underestimate the height of the OPA monolayer as the tip-sample interaction is strong enough to deform the flexible hydrocarbon chains of the OPA molecules [19,20]. Therefore, in order to estimate the height of the flexible organic monolayer, care should be taken as not to impose forces to the flexible OPA SAMs that might deform the molecular chains too much.

SE and SR data were collected from three spots each on the surface of a full-coverage OPA sample and a reference $\text{SiO}_2/\text{c-Si}$ substrate, respectively. Fig. 4 shows one set of the data of Δ , Ψ and reflectance spectra obtained on the two samples. Note that the wavelength of the light source for SE and SR is 245–1000 nm and 192–780 nm, respectively. As clearly shown in Fig. 4a, there is a significant decrease in Δ from the OPA sample compared with that from the reference $\text{SiO}_2/\text{c-Si}$ sample, indicating that SE has ample sensitivity for the OPA monolayer film to be detected. In contrast, there is little change in Ψ observed between the two samples. This is actually a typical case for an extremely thin dielectric film on a dielectric substrate, as the

change in ρ for such a system becomes imaginary, requiring change in Ψ to be near zero [9]. Therefore, the observed behaviors of Δ and Ψ suggest that the OPA monolayer film is extremely thin (as it should be) and transparent (i.e., non-absorbing) in visible range. In fact, as shown in Fig. 4b, there is no change in the reflectance between the OPA and the reference SiO₂/c-Si samples in visible range.

On the other hand, a decrease in reflectance for the OPA film sample compared with the reference SiO₂/c-Si sample is observed in Fig. 4b for light having wavelengths near 200 nm, suggesting that the OPA film becomes absorbing in deep-UV range. Those observations show that the presence of OPA monolayer on the SiO₂/c-Si substrate is readily detectable through the significant changes in Δ and that the OPA monolayer is a dielectric film with a possible optical band gap energy lying in deep-UV range.

Our OPA monolayer sample is modeled as stacks of OPA/SiO₂/c-Si. The SiO₂ thickness was deduced from Δ , Ψ and reflectance data measured on the reference SiO₂/c-Si substrate by adopting the optical functions from literature for the SiO₂/c-Si optical model [10], in which the only unknown was the thickness of the native oxide layer SiO₂. The thickness of the SiO₂ layer deduced from fitting the Δ , Ψ and reflectance data obtained on three spots of the reference silicon wafer using tabulated values [10] of n and k are 2.12, 2.09 and 2.15 nm, respectively (all of which have uncertainty less than 0.5%). Those values were coupled as inputs to represent the thickness of the SiO₂ layer in the optical stacks OPA/SiO₂/c-Si for the three sets of Δ , Ψ and reflectance data collected from three spots on the OPA sample. The advantage of using a silicon wafer as the substrate for an organic monolayer lies in the fact that optical properties of both the native oxide layer SiO₂ and the c-Si substrate are known so that the SiO₂ layer thickness can be precisely deduced from the Δ , Ψ and reflectance data [8,10].

Based on the observations of the dielectric nature of the OPA film in visible range and its becoming absorbing in deep-UV ranges, we adopt Tauc–Lorentz (TL) dispersion model developed by Jellison and Modine for parameterizing the dispersion of optical properties [21]. This dispersion model enforces the Kramers–Kronig (KK) consistency between n and k , which states that for physical properties that can be described with a complex function, the real and the imaginary parts are not independent to each other, but related through the KK integration. The TL model combines the Tauc joint density of states and a single transition Lorentz oscillator to account for interband absorption and bounded electron absorption, respectively. Dielectric function $\varepsilon = \varepsilon_1 + i\varepsilon_2$ and photon energy E are used in the TL dispersion model. The following equation of the TL dispersion model is for the imaginary part ε_2 accounting for the interband transition [21],

$$\varepsilon_2(E) = \left[\frac{AE_0C(E-E_g)^2}{(E^2-E_0^2)^2 + C^2E^2} \cdot \frac{1}{E} \right], E > E_g, \quad (2)$$

and $\varepsilon_2(E)=0, E \leq E_g$. The real part ε_1 is obtained by way of the KK integration,

$$\varepsilon_1(E) = \varepsilon_1(\infty) + \frac{2}{\pi} P \int_{E_g}^{\infty} \frac{\xi \varepsilon_2(\xi)}{\xi^2 - E^2} d\xi, \quad (3)$$

where P represents the Cauchy principal part of the integral, for which Jellison and Modine have shown a close solution [21,22]. The five parameters in Eqs. (2) and (3) are transition matrix element A , peak transition energy E_0 and broadening factor C of the Lorentz oscillator, the optical band gap E_g and a constant $\varepsilon_1(\infty)$ at high energy. With the OPA film thickness, we have six unknown parameters to deduce by fitting calculated values of Δ , Ψ and reflectance from the TL dispersion model to the data collected on the OPA sample surface. This dispersion model has been successfully applied to different types of films, both amorphous and crystalline [23–25]. Von Blanckenhagen et al. have demonstrated that the TL dispersion model can also be used to optical coating materials of dielectric metal oxides [26].

We treat our OPA SAM as an isotropic molecular film based on the fact that the molecules are dominated by methylene chains, which are unlikely to produce in-plane optical anisotropy as does a molecular film with unsaturated (π) bonds rich in the molecules [27]. We have examined octadecyltrichlorosilane SAM (this molecule has a silane headgroup and the exact same methylene chain as does an OPA molecule) prepared on a silicon wafer and found no sign of difference due to different headgroups. This experimental result suggests that phosphonic acid headgroup does not contribute much towards the monolayer's optical properties as accessed from ellipsometry and

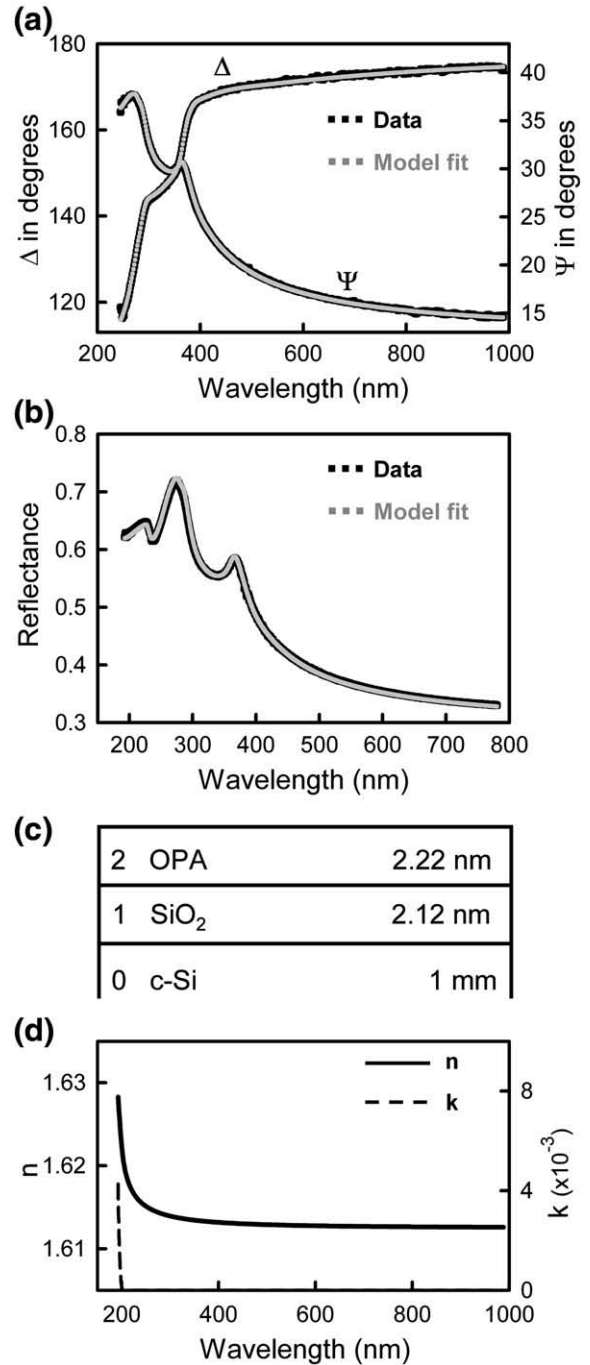


Fig. 5. Comparisons between one set of the data (black) and the calculated values (grey) of (a) Δ and Ψ and (b) reflectance based on the stack optical model of OPA/SiO₂/c-Si. Note that the black squares are plotted larger than the grey ones for clarity. The deduced thickness of OPA film and SiO₂ layer is shown in (c) with assumed c-Si substrate thickness. The dispersion of n and k deduced from multi-sample fitting on three spots for the OPA film is shown in (d).

reflectometry. With the TL dispersion model implemented in WVASE32, we deduce the five fitting parameters and the thickness for the OPA film through the best fitting to Δ , Ψ and reflectance data. For the OPA sample modeled as stacks of OPA/SiO₂/c-Si, the TL dispersion model calculated Δ , Ψ and reflectance values accounting for contributions from the OPA film, along with the trial OPA film thickness, the predetermined SiO₂ thickness, the contributions from SiO₂ and c-Si as calculated from their known tabulated values of n and k , as well as the thickness for those two stacks are fitted simultaneously to the three sets of Δ , Ψ and reflectance data obtained on the three spots on the OPA sample. An excellent fit was achieved with an MSE of 4.68. Comparisons between SE data obtained on one of the three spots on the OPA sample surface and the simulated values of Δ and Ψ are shown in Fig. 5a. The comparison between the reflectance simulation and the data from the same spot is shown in Fig. 5b. As clearly shown in Fig. 5a and b, we obtained excellent fitting between the simulation and the data. No surface roughness layer was necessary in our fitting since the silicon wafer and the OPA film possessed a roughness of only ~0.06 nm. The five fitting parameters are $A=5.56$ eV, $E_0=6.68$ eV, $C=0.73$ eV, $E_g=6.11$ eV and $\epsilon_1(\infty)=2.59$. Dispersion of n and k are calculated from that of the dielectric function by $\epsilon_1+i\epsilon_2=(n+ik)^2$. Note that we adopted the multi-sample fitting approach so that the parameters for n and k dispersions are the same for all of data from the three different spots on the OPA surface.

Another fitting parameter, the thickness of the OPA film, is deduced to be 2.22 nm (Fig. 5c) for one of the three spots. The other two values for the OPA film thickness deduced from the other two spots are 1.97 and 1.99 nm, respectively. Uncertainty for those estimated OPA thickness is less than 0.5%. The average OPA monolayer thickness (2.06±0.14 nm) deduced from fitting the TL dispersion model to the Δ , Ψ and reflectance data collected on three different spots agrees quite well with that (1.9±0.1 nm) measured by AFM on partial coverage OPA samples. The thickness of OPA monolayer deduced from the SE and SR data suggests OPA molecules are tilted approximately 35° away from normal direction as the molecule is believed to be 2.5 nm in length when fully extended [18]. Also shown in Fig. 5c is the thickness of SiO₂, which is deduced from the SE and SR data obtained on one of the three spots on the reference silicon wafer sample and used here as a fixed input. The c-Si layer is assumed to be 1 mm so that the light reflected from its backside is ignored.

Shown in Fig. 5d is deduced dispersion of n and k for the OPA monolayer film from SE and SR data with the TL dispersion model. It is clear that n of the OPA film comprised of hydrocarbon chains is featureless and k is zero in visible range, which is characteristic for transparent dielectric materials. The abrupt increase in k in deep-UV range for the OPA film hints that the film becomes absorbing in that photon energy range, which also results in an increase in n as required by the KK consistency. The deduced dispersion of k from the TL model for the OPA film appears to be typical for dielectric film [26]. The increase of k shown in Fig. 5d could be attributed to absorption of photon energy by the hydrocarbon chains of the OPA molecules through an electronic transition within the fundamental absorption band [28], which is 6.11 eV as deduced from the TL dispersion model.

It is known to be challenging to use the ellipsometric approach to deduce both the optical properties and thickness because they may display correlation. In order to assess the degree of correlation between the film thickness and the film optical properties, we tried purposely changing the OPA film thickness to test the fitting results. When inputting falsified OPA film thickness values of 1.0, 1.5, 3.0 and 4.0 nm, the fitting resulted in MSEs of 11.91, 6.72, 7.52, and 18.81, respectively. These MSE values obtained from falsified values for OPA film thickness deviate significantly from the MSE of 4.68 when the OPA film thickness is deduced from the best fit. It thus becomes clear that in the fitting process the correlation between the OPA film thickness and the optical properties is relatively weak. For example, the correlation coefficient between A (a measure of optical properties

as shown in Eq. (2)) and OPA film thickness is estimated to be $r=-0.73$ or $r^2=0.53$, when the falsified values of OPA film thickness were used in the fitting process as described above.

For our system of an OPA monolayer delivered on the native SiO₂ surface of a silicon wafer, we have been cautious in deducing the optical functions and film thickness. The steps we have taken to ensure the credibility of our analysis include (i) using the OPA thickness measured by AFM as the initial trial value for the OPA film thickness in fitting process; (ii) simultaneous SE and SR simulations on multi-sets of data obtained on OPA/SiO₂/c-Si sample to impose as many restrictions as possible to fitting conditions. Along with the AFM data for the film thickness, the well-known optical properties of silicon wafer and its native oxide layer are helpful in ensuring an accurate estimation of the optical properties of the OPA monolayer.

4. Conclusions

We have deduced optical functions and the thickness of a full-coverage OPA SAM spin-coated on the native SiO₂ surface of a single crystalline silicon substrate by adopting the TL dispersion model for the OPA monolayer film in optical stacks of OPA/SiO₂/c-Si for the sample system and fitting the model to multiple sets of SE and SR data collected on both the OPA/SiO₂/c-Si sample and the reference SiO₂/c-Si sample. The OPA monolayer is a dielectric film with an index of refraction of 1.61–1.62 in visible range and has an optical band gap of 6.11 eV in deep-UV range. The OPA thickness deduced (2.06±0.14 nm) from the dispersion model fitting is in good agreement with that measured by AFM (1.9±0.1 nm) on partial OPA monolayer samples.

Acknowledgements

We are grateful to H. Nakamura and K. Yoshino of Nanometrics Japan Ltd. for assistance in collecting the SE and SR data and G. Pribil of J. A. Woollam Co., Inc. for insightful discussion on optical modeling.

References

- [1] A. Ulman, Chem. Rev. 96 (1996) 1533.
- [2] R.G. Nuzzo, D.L. Allara, J. Am. Chem. Soc. 105 (1983) 4481.
- [3] R. Maoz, J. Sagiv, J. Colloid Interf. Sci. 100 (1984) 465.
- [4] E.L. Hanson, J. Schwartz, B. Nickel, N. Koch, M.F. Danisman, J. Am. Chem. Soc. 125 (2003) 16074.
- [5] H.-Y. Nie, M.J. Walzak, N. S. McIntyre, Langmuir 18 (2002) 2955.
- [6] H.-Y. Nie, M.J. Walzak, N. S. McIntyre, J. Phys. Chem. B 110 (2006) 21101.
- [7] H.-Y. Nie, N.S. McIntyre, W.M. Lau, Appl. Phys. Lett. 90 (2007) 203114.
- [8] D.E. Aspnes, A.A. Studna, Phys. Rev. B 27 (1983) 985.
- [9] H. Arwin, D.E. Aspnes, Thin Solid Films 138 (1986) 195.
- [10] C.M. Herzinger, B. Johs, W.A. McGahan, J.A. Woollam, W. Paulson, J. Appl. Phys. 83 (1998) 3323.
- [11] C.M. Herzinger, P.G. Snyder, B. Johs, J.A. Woollam, J. Appl. Phys. 77 (1995) 1715.
- [12] Y.H. Yang, J.R. Abelson, J. Vac. Sci. Technol. A 13 (1995) 1145.
- [13] H.G. Tompkins, W.A. McGahan, Spectroscopic Ellipsometry and Reflectometry: A User's Guide, Wiley, New York, 1999.
- [14] J.H. Bahng, M. Lee, H.L. Park, I.W. Kim, J.H. Jeong, K.J. Kim, Appl. Phys. Lett. 79 (2001) 1664.
- [15] G. Gonella, O. Cavalleri, I. Emiliano, L. Mattera, M. Canepa, R. Rolandi, Mater. Sci. Eng. C 22 (2002) 359.
- [16] D. Poelman, P.F. Smet, J. Phys. D: Appl. Phys. 36 (2003) 1850.
- [17] R.A.M. Azzam, N.M. Bashara, Ellipsometry and Polarized Light, North Holland, Amsterdam, 1977.
- [18] J.T. Woodward, A. Ulman, D.K. Schwartz, Langmuir 12 (1996) 3626.
- [19] K.J. Tupper, R.J. Colton, D.W. Brenner, Langmuir 10 (1994) 2041.
- [20] T. Bonner, A. Baratoff, Surf. Sci. 377–379 (1997) 1082.
- [21] G.E. Jellison, F.A. Modine, Appl. Phys. Lett. 69 (1996) 371.
- [22] G.E. Jellison, F.A. Modine, Appl. Phys. Lett. 69 (1996) 2137.
- [23] D. Amans, S. Callard, A. Gagnaire, J. Joseph, J. Appl. Phys. 93 (2003) 4173.
- [24] A.F.I. Morral, P.R.I. Cabarrocas, C. Clerc, Phys. Rev. B 69 (2004) 125307.
- [25] T. Easwarakhanthan, D. Beyssen, L. Le Brizoual, P. Anot, J. Appl. Phys. 101 (2007) 073102.
- [26] B. von Blanckenhagen, D. Tonova, J. Ullmann, Appl. Optics 41 (2002) 3137.
- [27] O.D. Gordan, M. Friedrich, D.R.T. Zahn, Thin Solid Films 455–456 (2004) 551.
- [28] M. Fox, Optical Properties of Solids, Oxford University, Oxford, 2001.